

## Assessment of the potential of MERIS near-infrared water vapour products to correct ASAR interferometric measurements

Z. LI\*†, J.-P. MULLER†, P. CROSS†, P. ALBERT‡, J. FISCHER‡ and  
R. BENNARTZ§

†Department of Geomatic Engineering, University College London, Gower Street,  
London WC1E 6BT, UK

‡Institut für Weltraumwissenschaften, Freie Universität Berlin, Carl-Heinrich-Becker-  
Weg 6-10, 12165 Berlin, Germany

§Atmospheric and Oceanic Sciences, University of Wisconsin-Madison, 1225 W. Dayton  
Street, Madison, WI 53706, USA

(Received 11 May 2004; in final form 9 August 2005)

Atmospheric water vapour is a major limitation for high precision Interferometric Synthetic Aperture Radar (InSAR) applications due to its significant impact on microwave signals. We propose a statistical criterion to test whether an independent water vapour product can reduce water vapour effects on InSAR interferograms, and assess the potential of the Medium Resolution Imaging Spectrometer (MERIS) near-infrared water vapour products for correcting Advanced SAR (ASAR) data. Spatio-temporal comparisons show *c.* 1.1 mm agreement between MERIS and GPS/radiosonde water vapour products in terms of standard deviations. One major limitation with the use of MERIS water vapour products is the frequency of cloud free conditions. Our analysis indicates that in spite of the low global cloud free conditions (~25%), the frequency can be much higher for certain areas such as Eastern Tibet (~38%) and Southern California (~48%). This suggests that MERIS water vapour products show potential for correcting ASAR interferometric measurements in certain regions.

### 1. Introduction

Tropospheric delay (especially the wet delay part due to water vapour) in radio signal propagation is known to be a major source of error for Interferometric Synthetic Aperture Radar (InSAR). The impact on SAR products such as topography and surface deformation has previously been estimated by several authors (Zebker *et al.* 1997, Williams *et al.* 1998). A 20% spatial or temporal change in relative humidity was estimated to cause between 80 m and 290 m of topographic error for baselines between 400 m and 100 m respectively, and an error of the order of 10–14 cm in the case of deformation estimates (Zebker *et al.* 1997). In this sense, knowledge of atmospheric water vapour is an important prerequisite for high precision InSAR applications, which is the principal motivation for this study.

The Medium Resolution Imaging Spectrometer (MERIS) was launched together with the Advanced Synthetic Aperture Radar (ASAR) on the ESA ENVISAT spacecraft on 1 March 2002. MERIS is a 68.5° field-of-view push-broom imaging

---

\*Corresponding author. Email: zhli@ge.ucl.ac.uk

spectrometer that measures the solar radiation reflected by the Earth and provides global coverage of the Earth every 3 days. Although MERIS is primarily dedicated to ocean biology and marine water quality, it also makes contributions to atmospheric and land surface related studies (ESA 2002b). MERIS has 2 out of 15 narrow spectral channels in the near-infrared, which allow for the remote sensing of Precipitable Water Vapour (PWV). These two channels are centred at 885 nm and 900 nm respectively, with a spectral bandwidth of 10 nm (Bennartz and Fischer 2001). MERIS near-infrared water vapour products are available at two spatial resolutions. In full resolution (FR) mode each pixel has an instantaneous field-of-view of  $0.019^\circ$ , with a nadir spatial sampling of 260 m across track by 290 m along track. In reduced resolution (RR) mode each pixel is approximately 1.04 km across track by 1.2 km along track at nadir.

Although MERIS and ASAR are operated independently, these two datasets can be acquired simultaneously and overlap with one another's fields-of-view during the daytime. In this study, we assess the accuracy requirement of independent datasets to reduce atmospheric effects on Synthetic Aperture Radar (SAR) interferograms and seek to understand the potential and limitations of MERIS near-infrared water vapour products to correct atmospheric effects in ASAR interferometric measurements.

An analysis of atmospheric effects on SAR interferograms is made, and a statistical criterion is proposed to assess whether independent water vapour products are sufficiently accurate to reduce atmospheric effects. A short description of radiosonde (RS), Global Positioning System (GPS) and MERIS datasets used in this paper is then given followed by spatio-temporal comparisons between RS, GPS and MERIS water vapour products. The frequency and percentage of cloud free conditions are evaluated for a number of geographical regions to assess the potential of MERIS to correct ASAR interferograms around the world. Finally, the results are discussed together with the conclusions reached.

## 2. Atmospheric effects on SAR interferograms

Numerous studies published in recent years illustrate that repeat-pass InSAR measurements are affected significantly by atmospheric water vapour. Interested readers should refer to Zebker *et al.* (1997) and Williams *et al.* (1998). For reference, the basic mathematical models for repeat-pass InSAR are as follows (Zebker *et al.* 1997):

$$\varphi = \frac{4\pi}{\lambda} \delta\rho \quad (1)$$

where  $\varphi$  is the measured interferometric phase (in radians),  $\lambda$  is the wavelength of the radar signal (in mm, e.g. *c.* 56.6 mm for ERS-1/2 and *c.* 56.3 mm for ASAR), and  $\delta\rho$  is the extra path length (in mm) of the SAR sensors' second pass relative to the first pass, which results in a phase shift.

### 2.1 Atmospheric effects on SAR interferograms—theory

From equation (1), taking into account the incidence angle of the radar signals, the total two-way phase delay due to water vapour for side-looking imaging radars can be given by:

$$\Delta\varphi = \frac{4\pi ZWD}{\lambda \cos\theta_{inc}} \quad (2)$$

where  $\Delta\varphi$  is the phase shift (in radians) due to water vapour for the radar echo signal

received from a point at an incidence angle  $\theta_{inc}$ , and  $ZWD$  represents Zenith Wet Delay (in mm), i.e. the path delay induced by water vapour along the zenith direction. The conversion factor of  $ZWD/PWV$  usually varies from 6.0 to 6.5, and is assumed to be 6.2 in this paper (Bevis *et al.* 1992, Niell *et al.* 2001, Li *et al.* 2003). The incidence angle of ASAR varies from  $15.0^\circ$  to  $45.2^\circ$  at an average satellite altitude of 786 km (ESA 2002a). In this paper, a nominal incidence angle of  $30^\circ$  is assumed, though a few special cases are explicitly identified in the text. It should be noted that water vapour effects on phase shifts will increase with the incidence angle.

For repeat-pass InSAR, considering that the phase of an interferogram is the difference of phase between two different SAR images collected at time  $t_1$  and  $t_2$  respectively, and assuming a standard deviation of  $\sigma_{ZWD}$  (in mm) on each  $ZWD$  measurement (i.e.  $\sigma_{ZWD,t_1} = \sigma_{ZWD,t_2} = \sigma_{ZWD}$ ), the effect of  $ZWD$  on interferograms can be given by:

$$\begin{aligned} \sigma_\varphi &= \left( \frac{4\pi}{\lambda} \frac{1}{\cos \theta_{inc}} \right)^2 \sqrt{\left( \sigma_{ZWD,t_1}^2 + \sigma_{ZWD,t_2}^2 \right)} \\ &= \frac{4\sqrt{2}\pi}{\lambda} \frac{1}{\cos \theta_{inc}} \sigma_{ZWD} \end{aligned} \tag{3}$$

One should keep in mind that equation (3) is based on the assumption that  $ZWD$  values are uncorrelated for different SAR images when their time interval is greater than 1 day. This has been demonstrated in previous work (e.g. Emdarson *et al.* 2003). From equation (3), an uncertainty of 1.0 mm in PWV ( $\sim 6.2$  mm in  $ZWD$ ) could result in an uncertainty of 0.4 fringes (i.e. a  $2\pi$  phase shift) in the resultant interferograms.

For repeat-pass topography mapping, taking into account the definition of the ambiguity height  $h_a$  (in metres), i.e. the amount of height change resulting in a phase change of one fringe (Rosen *et al.* 2000), the height error  $\sigma_h$  (in metres) with respect to  $ZWD$  error can be given by:

$$\sigma_h = \frac{h_a}{2\pi} \sigma_\varphi = \frac{2\sqrt{2}}{\lambda} \frac{h_a}{\cos \theta_{inc}} \sigma_{ZWD} \tag{4}$$

In order to derive a height accuracy better than 20 m, the uncertainty of  $ZWD$  should be less than 7.7 mm ( $\sim 1.2$  mm of PWV) with an ambiguity height of 45 m (i.e. a perpendicular baseline of 200 m). From equation (4), it is obvious that  $ZWD$  with a larger uncertainty can still meet this goal when used with a smaller ambiguity height. For example, the uncertainty of  $ZWD$  could be up to 15.8 mm ( $\sim 2.5$  mm of PWV) with an ambiguity height of 22 m (i.e. a perpendicular baseline of 400 m). However, it should be noted that the coherence of the radar echoes decreases when the baseline increases (i.e. baseline decorrelation) (Zebker and Villasenor 1992).

For repeat-pass deformation mapping, bearing in mind equation (16) of Zebker *et al.* (1997), the deformation error  $\sigma_\rho$  (in mm) with respect to  $ZWD$  error can be given by:

$$\sigma_\rho = \frac{\sqrt{2}}{\cos \theta_{inc}} \sigma_{ZWD} \tag{5}$$

When a deformation of 1 cm is required,  $ZWD$  with an uncertainty of 6.1 mm

(~1.0 mm of PWV) is needed. From equation (5), it can be seen that a smaller incidence angle would reduce atmospheric effects on surface deformation.

## 2.2 Phase variation on SAR interferograms and water vapour variation

In this paper, the variance statistic is used to describe the spatial variation of the observations in a two-dimensional field such as water vapour and SAR interferograms.

For a random function  $x$ , the variance is defined as (Hanssen 2001):

$$\begin{aligned}\sigma_x^2 &= \text{Var}(x) \\ &= \langle [x - \mu(x)]^2 \rangle\end{aligned}\quad (6)$$

where the angle brackets denote the expectation value, and  $\mu(x)$  represents the mean of  $x$ . For a SAR interferogram, its phase variation can be expressed as:

$$\begin{aligned}\sigma_{int}^2 &= \text{Var}(\Delta\rho) \\ &= \langle [\Delta\rho - \mu(\Delta\rho)]^2 \rangle\end{aligned}\quad (7)$$

where  $\Delta\rho$  represents range change in the satellite line of sight (in mm). It should be noted that the unwrapped phases of the interferogram are converted to range changes using equation (1).

For a specific water vapour field, the variance of its induced Zenith Wet Delays ( $ZWD$ , in mm) can be written as:

$$\begin{aligned}\sigma_{ZWD}^2 &= \text{Var}(ZWD) \\ &= \langle [ZWD - \mu(ZWD)]^2 \rangle\end{aligned}\quad (8)$$

Since the phase of an interferogram is the difference of phase between two different SAR images, what matters to an interferogram is the change in  $ZWD$  from scene to scene rather than the absolute value of  $ZWD$  itself. In order to reduce water vapour effects on interferograms, a Zenith Path Delay Difference Map (ZPDDM) should be produced by differencing the  $ZWD$  values derived from the two different water vapour fields (Li *et al.* 2005). Assuming  $ZPDDM = ZWD_{t_2} - ZWD_{t_1}$ , where  $t_1$  and  $t_2$  are the observation times of the water vapour fields, the variance of the ZPDDM can be given as:

$$\begin{aligned}\sigma_{ZPDDM}^2 &= \text{Var}(ZPDDM) \\ &= \text{Var}(ZWD_{t_2} - ZWD_{t_1})\end{aligned}\quad (9)$$

Taking into account the fact that  $ZWD$  values are uncorrelated when their observation interval is greater than 1 day (Emardson *et al.* 2003), equation (9) can be re-written as:

$$\begin{aligned}\sigma_{ZPDDM}^2 &= \text{Var}(ZWD_{t_2} - ZWD_{t_1}) \\ &= \text{Var}(ZWD_{t_2}) + \text{Var}(ZWD_{t_1}) \\ &= \sigma_{ZWD_{t_2}}^2 + \sigma_{ZWD_{t_1}}^2\end{aligned}\quad (10)$$

From equation (10), it is clear that the variance of  $ZWD$  values in the Zenith Path

Delay Difference Map (ZPDDM) could be derived directly from the corresponding two water vapour fields (instead of the ZPDDM itself).

### 2.3 Statistical criterion for water vapour correction

As a means of measurement, each technique (including MERIS) has its own inherent limitations that restrict the accuracy of its water vapour products. Moreover, the spatial variations of water vapour change with time, which leads to phase shifts on SAR interferograms. So a question arises: Under what condition(s) are MERIS near-infrared water vapour products sufficiently accurate to reduce water vapour effects on ASAR measurements? In order to answer the question fully, a statistical criterion for the correction of ASAR measurements by the use of MERIS near-infrared water vapour is proposed:

- (1) Calculate the phase variation  $\sigma_{int}^2$  for the specific interferogram using equation (7). It should be noted that: (a) a precise Digital Elevation Model (DEM) such as that from the Shuttle Radar Topography Mission (SRTM) should be used to remove the topographic contributions on the interferogram, so that the phase remaining should be almost entirely due to atmospheric effects and deformation between the two acquisitions of SAR images; (b) the area(s) with known and evident deformation signals should be masked manually; (c) range changes (in mm), instead of unwrapped phases (in radians), should be used in equation (7);
- (2) Calculate the spatial variation  $\sigma_{ZPDDM}^2$  of ZWD values in the ZPDDM using equation (10) with two MERIS near-infrared water vapour fields. It should be noted that: (a) only the water vapour retrievals under cloud free conditions can be used; (b) PWV values should be converted to ZWD using surface temperature (Bevis *et al.* 1992);
- (3) Map  $\sigma_{ZPDDM}^2$  from the zenith direction to the satellite line of sight:  $\sigma_{SPDDM}^2 = \sigma_{ZPDDM}^2 / \cos^2 \theta_{inc}$ , where SPDDM represents the Slant Path Delay Difference Map, and  $\theta_{inc}$  is the incidence angle of radar signals;
- (4) Compare  $\sigma_{SPDDM}^2$  with  $\sigma_{int}^2$ . If  $\sigma_{SPDDM}^2 < \sigma_{int}^2$ , then the ZPDDM can be used to remove the long-wavelength water vapour effects on ASAR measurements. Otherwise, these two corresponding water vapour fields cannot safely be applied to ASAR atmospheric correction, because the uncertainty in the ZPDDM, inherited from MERIS near-infrared water vapour products, will corrupt the radar signals if the ZPDDM is applied.

## 3. Spatio-temporal comparisons between RS, GPS and MERIS water vapour products

### 3.1 Data descriptions

**3.1.1 Radiosondes (RS).** Ten Vaisala RS-80 radiosonde stations, with launches twice daily or more often, and distributed around Germany, were used in this study (figure 1). RS data consist of height profiles for pressure, temperature and dew point. As these profiles contain heights only at mandatory levels, and much higher resolution is given for the meteorological variables, values of the missing heights were calculated from reported temperature and pressure using the hypsometric equation (Li *et al.* 2003). Radiosondes are expected to produce PWV with an uncertainty of 1–2 mm, which is considered to be the accuracy standard of PWV for

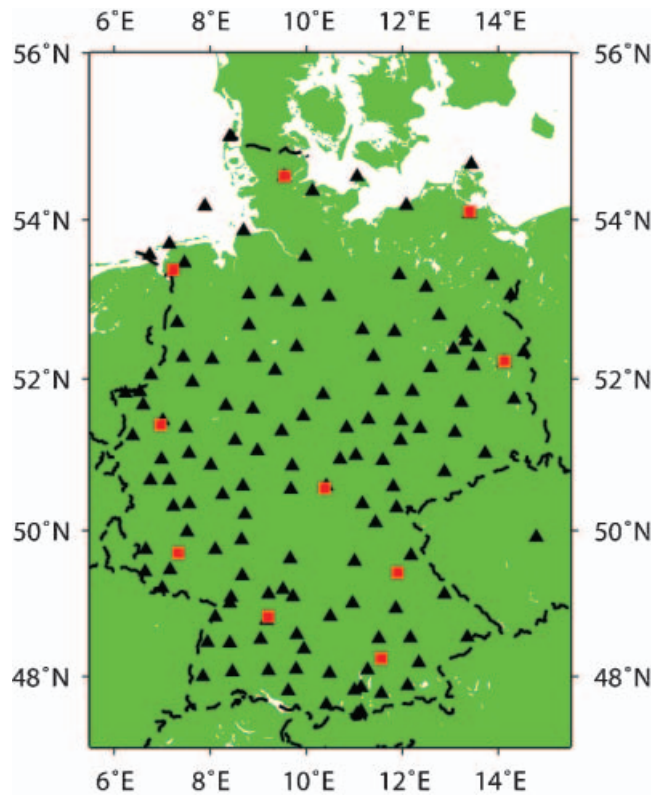


Figure 1. Radiosonde and GPS stations across Germany. Red solid squares represent radiosonde stations, and black solid triangles represent GPS stations.

meteorologists (Niell *et al.* 2001). In this study, RS data were processed to derive Zenith Wet Delay (ZWD) using a ray tracing program developed by J. Davis, T. Herring and A. Niell of MIT (Niell *et al.* 2001), and ZWDs were converted into PWVs using surface temperature (Bevis *et al.* 1992).

**3.1.2 GPS.** Near real-time GPS PWV retrievals from the GeoForschungsZentrum Potsdam (GFZ) were used in this study. The GPS Atmosphere Sounding Project (GASP), led by GFZ, utilizes a dense GPS network with more than 120 sites all over Germany with an average spacing of about 50 km (see figure 1). Comparisons with post-processed results as well as validation with independent techniques and models showed that a standard deviation of better than 1 mm in the PWV estimates could be achieved (Reigber *et al.* 2002).

**3.1.3 MERIS.** The MERIS near-infrared water vapour retrieval algorithm relies on observations of water vapour absorption of near-infrared solar radiation reflected by land, water surfaces and clouds. Based on the assumption that an exponential relationship exists between the absorber mass and extinction, PWV can be derived from the ratio of measured radiances in the water vapour absorbing channel at 900 nm and in the atmospheric window channel at 885 nm above both land and ocean surfaces under cloud free conditions (Bennartz and Fischer 2001). When there are clouds, PWV above the highest cloud level can be derived (Albert *et al.* 2001).

Since repeat-pass InSAR is applied to produce DEMs and deformation maps, only MERIS near-infrared water vapour products over land were investigated in this study. The theoretical accuracy of the algorithm is 1.6 mm under cloud free conditions over land (Bennartz and Fischer 2001). A preliminary validation of the algorithm was performed with data from the Modular Optoelectronic Scanner (MOS) data. The algorithm results were compared with radio soundings, and a Root Mean-Square Error (RMSE) of 2.49 mm with a bias of 0.04 mm was observed (Bennartz and Fischer 2001). The MERIS breadboard algorithm developed at the Freie Universität Berlin (FUB) was used to process the reduced resolution (RR) raw level 1 data provided by ESA/ESRIN. The reduced resolution (RR) data used in this paper covered the time period from October 2002 to September 2003.

### 3.2 *Spatio-temporal comparisons between RS, GPS and MERIS water vapour products*

In order to assess the performance of MERIS for measuring water vapour, spatio-temporal comparisons between radiosondes (RS), GPS and MERIS water vapour products were performed and are reported in this paper. Spatio-temporal comparisons here involved all the coincident observations collected over each and every station (RS or GPS) during the experiment period. Comparisons were made station by station. As MERIS near-infrared water vapour is sensitive to the presence of clouds in the field-of-view, only the MERIS PWV estimates collected under clear sky conditions were selected using a cloud mask produced by the FUB for this study (Rene Preusker, personal communication, 2004). Note that all statistics are given after  $2\sigma$  elimination, i.e. all differences more than twice the standard deviation were considered to be outliers and were removed. This elimination was mainly needed where poor collocations between the data in either time or space (e.g. a time difference between different datasets of up to 1.5 hours in the comparison between RS and MERIS, see below) were found, or where cloudy pixels were falsely identified as cloud free.

Vaisala RS-80 radiosonde data and MERIS near-infrared water vapour products collected over Germany were compared with each other. In addition to the requirement of cloud free conditions, RS data were chosen only if the time difference between a MERIS overpass and a RS launch was less than 1.5 hours. There were 315 coincident RS and MERIS observations available in total, and 34 cases were omitted due to the  $2\sigma$  exclusion (figure 1(a)). Assuming the relationship between MERIS and RS PWV to be linear,  $\text{MERIS-PWV} = a \times (\text{RS-PWV}) + b$ , a least squares fit gave a scale factor of  $1.09 \pm 0.01$  with a zero-point offset of  $-0.4 \pm 0.1$  mm and a standard deviation of 1.1 mm. The mean difference (MERIS – RS) PWV was 0.7 mm with a standard deviation of 1.4 mm.

The criteria applied to choose GPS observations were different to those applied to RS. Since GPS made continuous observations and PWV was estimated with a resolution of 30 minutes, GPS data covering the scan time of MERIS measurements were selected, and so the time difference was much smaller than that between MERIS and RS. The spatial distribution of the GPS sites is much denser than that of the RS sites; therefore the number of coincident GPS and MERIS observations was greater than that of RS and MERIS observations. There were 2261 cases available and 123 cases were omitted due to the  $2\sigma$  exclusion. The correlation coefficient between MERIS and GPS PWV was 0.99 (figure 1(b)). The average difference (MERIS – GPS) PWV was  $-0.2$  mm with a standard deviation of 1.1 mm.

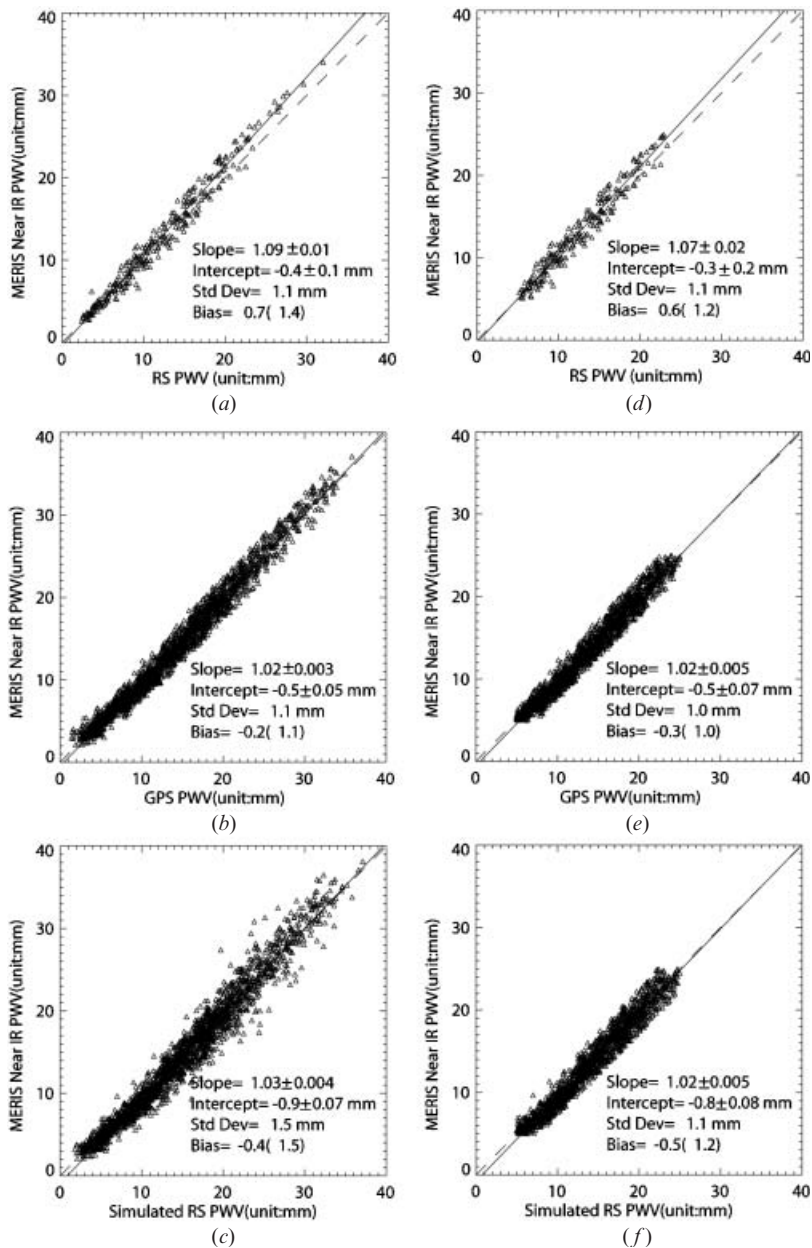


Figure 2. (a) Scatter plots of MERIS-PWV and RS-PWV under cloud-free conditions. The line of perfect fit (dashed line) and a least squares regression line (solid line) are plotted. The number of valid samples was 281, and 34 were omitted due to the  $2\sigma$  exclusion. (b) Scatter plots of MERIS-PWV and GPS-PWV under cloud-free conditions. The number of valid samples was 2138, and 123 were omitted. (c) Scatter plots of MERIS-PWV and simulated RS-PWV under cloud-free conditions. The RS-PWV values were simulated using the GPS-PWV values at the nominal launch time of RS, i.e. 11 UTM, with observation intervals of 30 minutes. (d) Scatter plots of MERIS-PWV and RS-PWV under moderate conditions with clear sky (PWV: 5–25 mm). The number of valid samples was 217, and 25 were omitted. (e) Scatter plots of MERIS-PWV and GPS-PWV under moderate conditions with clear sky (PWV: 5–25 mm). The number of valid samples was 1654, and 106 were omitted. (f) Scatter plots of MERIS-PWV and simulated RS-PWV under moderate conditions with clear sky (PWV: 5–25 mm).

A linear fit of MERIS–PWV to GPS–PWV yielded a relationship of  $\text{MERIS–PWV} = 1.02(\pm 0.003) \times (\text{GPS–PWV}) - 0.5(\pm 0.05)$ .

In order to validate the MERIS near-infrared water vapour products under different conditions, such as dry, moderate or wet conditions, inter-comparisons between GPS and MERIS PWV were performed in different seasons (table 1). It is clear that it was wettest in the summer with a mean PWV of 21.4 mm and driest in the winter with a mean PWV of 5.4 mm. Except for the inter-comparison in the winter, the others showed scale factors greater than unity and negative zero-point offsets. The inter-comparison in the winter showed an apparently worse agreement in terms of a correlation of 0.89, although a positive offset at zero, a scale factor of significantly less than unity, and the limited range of PWV resulted in a small standard deviation of 0.8 mm. Given the error characteristics of MERIS PWV retrievals (Bennartz and Fischer 2001), the large difference in the winter is most likely to be due to the high solar zenith angles. The inter-comparison in the summer showed a larger scale factor and a larger offset from zero. These results suggest that MERIS PWV values were slightly greater than GPS values under both dry and wet conditions for the dataset used in the paper.

Supposing that PWV varied from 5 to 25 mm under moderate conditions (which is similar to autumn), a linear fit of MERIS–PWV to GPS–PWV yielded a relationship of  $\text{MERIS–PWV} = 1.02(\pm 0.005) \times (\text{GPS–PWV}) - 0.5(\pm 0.07)$  with a standard deviation of 1.0 mm (table 1, figure 1(e)). A similar inter-comparison was performed between MERIS and RS PWV (figure 1(d)). The MERIS PWV values were  $1.07 \pm 0.02$  times the RS PWV with a zero-point offset of  $-0.3 \pm 0.2$ .

It should be noted that the standard deviations of all of the above inter-comparisons are smaller than the quadratic sum of both the accuracy of GPS PWV (1–2 mm, or more for RS PWV) and the theoretical accuracy of MERIS PWV ( $\sim 1.6$  mm), and thus the agreement between GPS (or RS) and MERIS PWV is significantly better than those estimated from the accuracy of each technique.

It should also be noted that the scale factors of MERIS/RS were larger than those of MERIS/GPS in figure 1. On the one hand, in order to check the effects of the time difference between RS and MERIS measurements, RS PWV values were simulated

Table 1. Seasonal inter-comparisons between Medium Resolution Imaging Spectrometer (MERIS) and Global Positioning System (GPS) Precipitable Water Vapour (PWV) across Germany.

Season <sup>a</sup>	Number of passes <sup>b</sup>	$a^c$	$b^c$ (mm)	Correlation	PWV range (mm) <sup>d</sup>	Mean PWV (mm) <sup>d</sup>	StdDev (mm) <sup>e</sup>
Spring	879(61)	$1.02 \pm 0.006$	$-0.6 \pm 0.07$	0.98	[1.5, 33.5]	11.2	1.0
Summer	707(34)	$1.06 \pm 0.009$	$-1.4 \pm 0.20$	0.97	[5.5, 35.8]	21.4	1.3
Autumn	394(20)	$1.06 \pm 0.010$	$-0.9 \pm 0.20$	0.97	[5.0, 26.9]	14.8	1.0
Winter	156(10)	$0.89 \pm 0.020$	$0.8 \pm 0.10$	0.89	[1.4, 17.0]	5.4	0.8
All	2138(123)	$1.02 \pm 0.003$	$-0.5 \pm 0.05$	0.99	[1.4, 35.8]	14.7	1.1
[5, 25]	1654(106)	$1.02 \pm 0.005$	$-0.5 \pm 0.07$	0.98	[5.0, 25.0]	14.2	1.0

<sup>a</sup>Spring: March–May 2003; Summer: June–August 2003; Autumn: October–November 2002 and September 2003; Winter: December 2002–February 2003.

<sup>b</sup>The number of valid passes (the number of samples omitted due to the  $2\sigma$  exclusion).

<sup>c</sup>Here  $\text{MERIS–PWV} = a \times (\text{GPS–PWV}) + b$ .

<sup>d</sup>Derived from GPS measurements.

<sup>e</sup>Standard deviation of differences (MERIS–PWV – GPS–PWV).

using GPS PWV estimates at the nominal launch time (i.e. 11 UTM) with observation intervals of 30 minutes (from 11:00 UTM to 11:30 UTM). An inter-comparison between the simulated RS PWV values and the 'real' GPS PWV values (which overlapped with the MERIS overpasses) showed that the simulated values were  $0.99 \pm 0.003$  times the 'real' GPS PWV values with a zero-point offset of  $0.5 \pm 0.04$  and a standard deviation of 0.9 mm (not shown). Relative to the 'real' GPS PWV values in figure 1(b) and (e) respectively, both scatter plots between MERIS and simulated RS PWV in figure 1(c) and (f) showed larger standard deviations and larger mean differences with similar scale factors, suggesting that the time difference made contributions to the larger standard deviations, but had no significant effects on the larger scale factor of MERIS/RS. On the other hand, bearing in mind that the scale factor of RS/GPS was  $\sim 0.95$  for Vaisala RS-80 radiosondes (Niell *et al.* 2001, Li *et al.* 2003), the division of the scale factors of MERIS/GPS (1.03) and RS/GPS (0.95) was about 1.08 within  $1\sigma$  of the MERIS/RS scale factor (1.09), when using all the data sets (figure 1(a) and (c)). Under moderate conditions (figure 1(d) and (f)), the division of the scale factors of MERIS/GPS (1.02) and RS/GPS (0.95) was about 1.07, identical to the MERIS/RS scale factor (1.07). These imply that both types of inter-comparisons were consistent with each other.

#### 4. Statistics of cloud free conditions

Although PWV can be retrieved above the highest cloud level under cloudy conditions for MERIS (Albert *et al.* 2001), our interests here for InSAR applications lie in water vapour retrievals over land instead of clouds. Therefore, the frequency and the percentage of cloud free conditions are important and need to be evaluated. The frequency of cloud free conditions refers to the probability of cloud free occurrence; the percentage of cloud free conditions is inferred from the density of cloud free pixels. Wylie and Menzel (1999) investigated the frequency, geographical distribution, and seasonal changes of upper-tropospheric clouds using the High Resolution Infrared Radiation Sounder (HIRS) over 8 years (1989–1997) and reported that clear skies were found in 27% of all observations of the Earth from  $65^\circ$  S to  $65^\circ$  N latitude in the boreal summer (June–August) and in only 24% during the boreal winter (December–February). It should be noted that the spatial resolution of the cloud product derived from HIRS data is 20 km. Therefore, HIRS may observe broken clouds, overcast transmissive clouds, and/or broken transmissive clouds, which implies an observation where the HIRS radiometer detects radiation from below, as well as above a cloud layer (Wylie and Menzel 1999).

In this study, the 1 km cloud mask product stored in MODIS near IR water vapour product (Ackerman *et al.* 1998) has been utilized to produce the statistics of cloud free conditions.

##### 4.1 Frequency of cloud free conditions

An area of  $4^\circ \times 4^\circ$  in Germany ( $49\text{--}53^\circ$  N,  $8\text{--}12^\circ$  E) was chosen to estimate the frequency of cloud free conditions, and a uniformly spaced grid of  $1\text{ km} \times 1\text{ km}$  was applied. There were  $481 \times 481$  grid cells in total.

Figure 3 shows seasonal frequencies of cloud free conditions over parts of Germany during the period from 1 March 2002 to 28 February 2003. It is clear that the frequencies varied from place to place in all four figures. For example, the frequency in the south of the test area was higher than that in the centre.

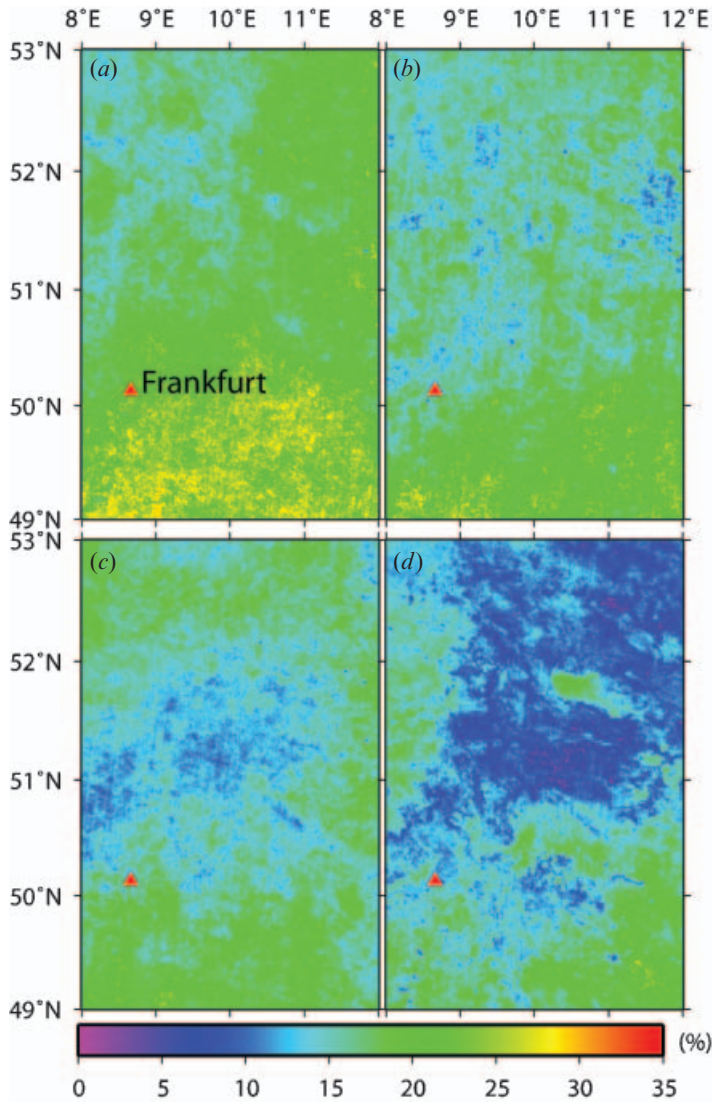


Figure 3. Seasonal frequencies of cloud free conditions over Central Germany during the period from 1 March 2002 to 28 February 2003. (a) Spring (March–May). (b) Summer (June–August). (c) Autumn (September–November). (d) Winter (December–February).

Table 2 shows a summary of seasonal frequency variation: both the highest individual and average frequencies over Germany were found in spring (33% and 19%, respectively) whilst the lowest occurred in winter (0% and 13%). The average frequency of cloud free conditions was found to be 17%, with a maximum of 25% in the area during the whole year.

Similar analyses were applied to a  $4^{\circ} \times 4^{\circ}$  region in Eastern Tibet during the period from 1 September 2001 to 31 August 2004 (table 2, figure 4). Contrary to Germany, both the lowest individual and average frequencies over the Eastern Tibet region were observed in summer (4% and 25%, respectively). The highest individual frequency was found in winter (77%) and the highest average frequency in autumn (46%). The average frequency of cloud free conditions was found to be 38%, with a

Table 2. Seasonal frequencies of cloud free conditions over Germany and the Eastern Tibet region.

Season	Germany (%)			Eastern Tibet (%)		
	Max	Min	Average	Max	Min	Average
Spring	33	7	19	62	9	36
Summer	32	4	18	51	4	25
Autumn	26	6	16	69	15	46
Winter	27	0	13	77	5	44
All	25	7	17	60	15	38

maximum of 60% in the Eastern Tibet region over the entire 3-year time period. This suggests that the Eastern Tibet region exhibits higher frequencies of cloud free conditions than Germany, which provides further evidence that the frequency varies from place to place.

#### 4.2 Percentage of cloud free conditions

The statistics were calculated as a percentage of cloud free observations relative to all of the observations in Germany during the period from 1 March 2002 to 28

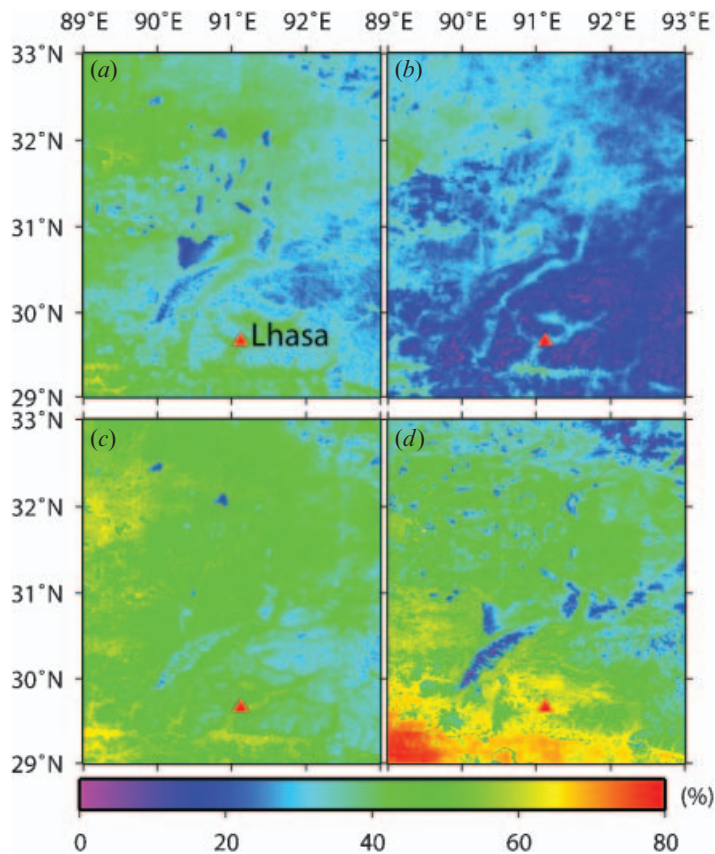


Figure 4. Seasonal frequencies of cloud free conditions over Eastern Tibet during the period from 1 September 2001 to 31 August 2004. (a) Spring (March–May). (b) Summer (June–August). (c) Autumn (September–November). (d) Winter (December–February).

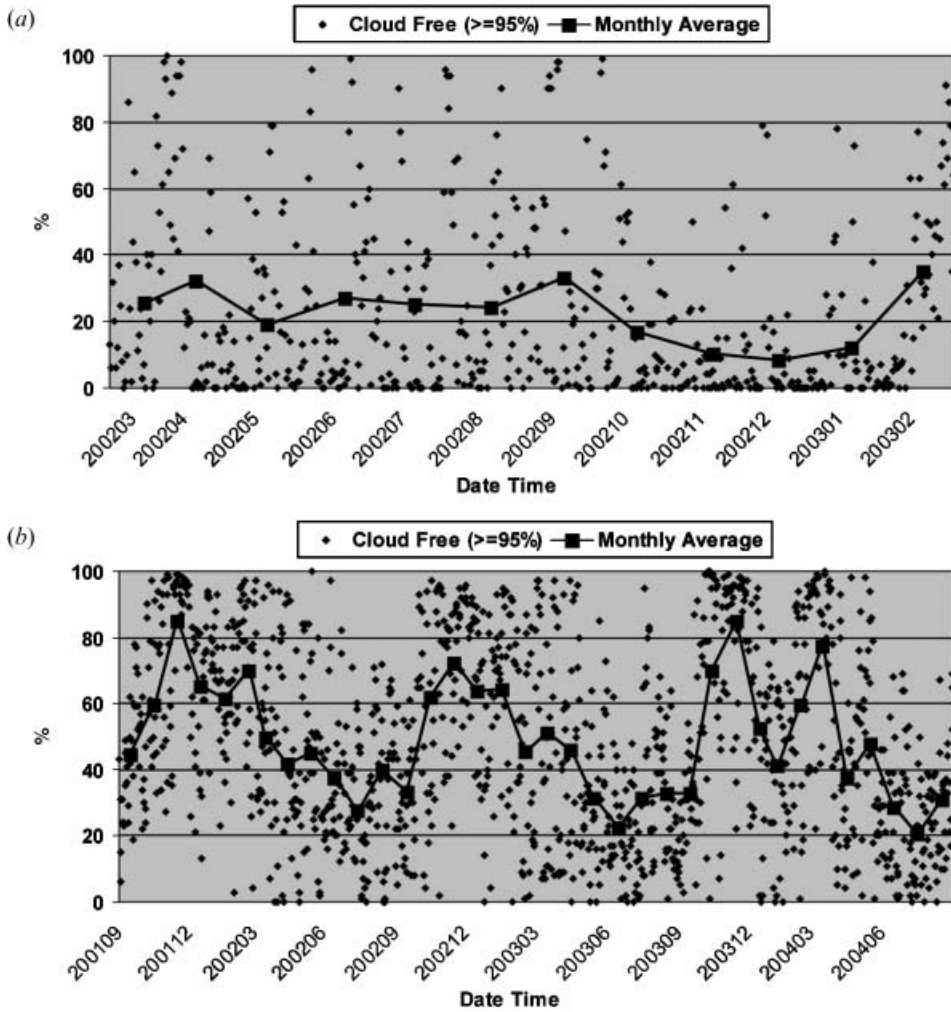


Figure 5. Statistics of percentage of cloud free conditions: (a) an area of  $4^\circ$  (latitude)  $\times$   $4^\circ$  (longitude) in Central Germany during the period from 1 March 2002 to 28 February 2003; (b) an area of  $4^\circ$  (latitude)  $\times$   $4^\circ$  (longitude) in Eastern Tibet during the period from 1 September 2001 to 31 August 2004.

February 2003. Figure 5(a) shows the percentage of cloud free conditions with a trend line showing monthly average values. It is obvious that the percentages of cloud free conditions varied widely, even from 0% to 100% on a day-to-day basis. A seasonal variation can also be observed, e.g. there are far fewer cloud free conditions in the late autumn and early winter in Germany. The average percentage was 22% during the experimental period.

Figure 5(b) shows the percentage of cloud free conditions over the Eastern Tibet region ( $29\text{--}33^\circ$  N,  $89\text{--}93^\circ$  E) with a monthly trend line. The monthly percentages were found to vary from 20% and 85% with an average of 49%. Comparing figures 5(a) and (b), it is clear that the trend line in the Eastern Tibet region was different to that in Germany, and the Eastern Tibet region had a relatively higher overall percentage. It is also obvious from figure 5(b) that the trend line varied from season to season, and from year to year.

## 5. Discussion and conclusions

The requirement for independent sources of data (e.g. MERIS near-infrared water vapour products) to correct ASAR measurements has been investigated. It has been found that PWV with an uncertainty of  $<1.0$  mm is needed to detect surface deformation of 1.0 cm using the repeat-pass method. In order to derive topography better than 20 m, PWV with an uncertainty of  $<1.2$  mm is needed for interferometric pairs with a perpendicular baseline of 200 m, i.e. an ambiguity height of 45 m.

To assess the potential for using MERIS near-infrared water vapour products to correct ASAR measurements, the MERIS near-infrared water vapour products processed at the Freie Universität Berlin (FUB) were evaluated using RS and GPS data. A comparison with Vaisala RS-80 radiosondes revealed a strong dry bias of RS measurements for high PWV values with a MERIS/RS scale factor of 1.09 when using the whole dataset, or 1.07 under moderate conditions, and with standard deviations of 1.4 mm and 1.2 mm, respectively. A simulation of RS PWV values using GPS data showed that the time difference between MERIS and RS could contribute to a larger standard deviation, but had no significant effects on scale factors. A comparison of MERIS and GPS PWV showed an excellent agreement with a standard deviation of 1.1 mm, which is well below the estimated accuracy of both techniques. The scatter plots (figure 1(a) and (b)) showed a slight curvature with positive biases for very low ( $\text{PWV} < 0.5$  mm) and very high ( $\text{PWV} > 25$  mm) PWV values, indicating that MERIS overestimated PWV against GPS under both very dry ( $\text{PWV} < 0.5$  mm, mainly in the winter) and very wet ( $\text{PWV} > 25$  mm, mainly in the summer) conditions. In the winter (i.e. under dry conditions), the high solar zenith angle may lead to a decrease of accuracy of the retrieved MERIS PWV values. However, in order to assess the accuracy of MERIS near-infrared water vapour products under dry/wet conditions, a larger dataset is needed. It should be noted that the standard deviations were very small (within 1.3 mm) in any case. Therefore, it is safe to infer that MERIS near-infrared water vapour has a better accuracy than the theoretical value (i.e. 1.6 mm), particularly under moderate conditions with PWV values ranging from 5 mm to 25 mm.

Assuming MERIS water vapour values are independent of each other for every pixel, a low pass filter with an average width of 2 pixels can improve the accuracy by a factor of 2 at the expense of the spatial resolution (degraded to 600 m for the full resolution water vapour product and 600 m for the reduced resolution water vapour product respectively). In this case, taking into account the requirements for correcting InSAR measurements (see §2.1), MERIS water vapour products can be used for InSAR atmospheric correction. This approach has been fully investigated using the NASA Terra Moderate Resolution Imaging Spectroradiometer (MODIS) data, and its application to ESA ERS-2 data over the Los Angeles region shows the use of MODIS near IR water vapour products not only helps discriminate geophysical signals from atmospheric artefacts, but also reduces water vapour effects significantly on interferograms (Li *et al.* 2005). The MODIS near-infrared water vapour product is claimed to be determined with an accuracy of 5–10% with a spatial resolution of 1 km, and errors will be greater for retrievals from data collected over dark surfaces or under hazy conditions (Gao and Kaufman 2003).

It appears that the MERIS correction model is much more advantageous to ASAR than the MODIS water vapour correction model is to ERS-2. First, a scale uncertainty of about 1.05 was observed in the Terra MODIS near IR water vapour product (collection 4), which indicates that at least one GPS station is required to

calibrate MODIS data (Li *et al.* 2005). However, since the MERIS/GPS scale was around 1.02 with a limited range of PWV values (e.g. mainly 0–40 mm in Europe (Reigber *et al.* 2002)), and the RMS difference between MERIS and GPS was 1.1 mm, which is well below the estimated accuracy of both techniques (see §3.2), GPS data are not required to calibrate MERIS data, particularly under moderate conditions. Secondly, the time difference between MODIS and ERS-2 data acquisitions can be up to 1 hour (Li *et al.* 2005). However, MERIS and ASAR are on board the same platform (ENVISAT), and they can collect observations simultaneously.

Since MERIS near-infrared water vapour is sensitive to the presence of clouds, and only PWV values above the land are applicable in this study, the frequency and percentage of cloud free conditions have been investigated. This has been carried out using data from Germany for 1 year and from the Eastern Tibet region in China for 3 years. The frequencies varied from place to place and the percentages from day to day. Seasonal variations were also observed, and the highest (and/or lowest) frequencies were found in different seasons for different places. It appears that the Eastern Tibet region had higher frequencies and percentages of cloud free conditions than Germany. Bearing in mind that the global cloud free conditions are about 25% (Menzel *et al.* 1996, Wylie *et al.* 1999), the low frequency of cloud free observations can be a major limitation in applying MERIS (and MODIS) near IR water vapour products to InSAR atmospheric correction. However, it has been shown that the frequency of cloud free conditions can, for some areas, be much higher than the global average, e.g. 38% for the Eastern Tibet region (see §4.1) and 48% for the SCIGN region (Li *et al.* 2005). This suggests that MERIS near-infrared water vapour products show promise for correcting ASAR measurements.

Given the accuracy and the cloud-free requirements, the benefits from MERIS near-infrared water vapour products appear to be as follows:

- (1) ASAR data selection. Atmospheric effects might be reduced by carefully selecting ASAR images with less water vapour variations as indicated by MERIS data.
- (2) Atmospheric effects assessment. MERIS PWV products can provide *a priori* knowledge of the degree of water vapour contamination in an interferogram, which will be helpful in separating real deformation information from tropospheric noise.
- (3) Water vapour correction under cloud free conditions. In order to suppress the inherent noise of MERIS near-infrared water vapour products, a low-pass filter with an average width of 2 pixels should be applied to water vapour fields (Li *et al.* 2005).

### Acknowledgments

This research was supported by an Overseas Research Students Award (ORS) and a UCL Graduate School Research Scholarship to Z. Li at University College London. This work was also partly supported by the EU-CLOUDMAP2 project (EVG1-CT-2000-00033), and partly carried out within the framework of the NERC Earth Observation Centre of Excellence: Centre for the Observation and Modelling of Earthquakes and Tectonics (COMET). We thank E. J. Fielding and A. Sibthorpe for useful discussions and the two anonymous referees for helpful suggestions. We

would like to express our appreciation to Professor C. Reigber, Dr G. Gendt and Dr Y. Liu for provision of the GFZ near real-time GPS water vapour products. The MERIS near-infrared water vapour L1 data were obtained from ESA under the HAZARDMAP data grant (ID 853), and RS data were courtesy of the British Atmospheric Data Centre (BADC, <http://badc.nerc.ac.uk>).

## References

- ACKERMAN, S., STRABALA, K., MENZEL, W., FREY, R., MOELLER, C. and GUMLEY, L., 1998, Discriminating clear sky from clouds with MODIS. *Journal of Geophysical Research*, **103**, pp. 32141–32157.
- ALBERT, P., BENNARTZ, R. and FISCHER, J., 2001, Remote sensing of atmospheric water vapor from backscattered sunlight in cloudy atmospheres. *Journal of Atmospheric and Oceanic Technology*, **18**, pp. 865–874.
- BENNARTZ, R. and FISCHER, J., 2001, Retrieval of columnar water vapour over land from back-scattered solar radiation using the Medium Resolution Imaging Spectrometer (MERIS). *Remote Sensing of Environment*, **78**, pp. 271–280.
- BEVIS, M., BUSINGER, S., HERRING, T., ROCKEN, C., ANTHES, R. and WARE, R., 1992, GPS meteorology: remote sensing of atmospheric water vapour using the Global Positioning System. *Journal of Geophysical Research*, **97**, pp. 15787–15801.
- EMARDSON, T., SIMONS, M. and WEBB, F., 2003, Neutral atmospheric delay in interferometric synthetic aperture radar applications: statistical description and mitigation. *Journal of Geophysical Research*, **108**, p. 2231, doi:10.1029/2002JB001781.
- ESA, 2002a, ASAR Product Handbook, Issue 1.1. Available online at: <http://envisat.esa.int/dataproducts/asar> (accessed 12 April 2004).
- ESA, 2002b, MERIS Product Handbook, Issue 1.1. Available online at: <http://envisat.esa.int/dataproducts/meris> (accessed 12 April 2004).
- GAO, B. and KAUFMAN, Y., 2003, Water vapor retrievals using Moderate Resolution Imaging Spectroradiometer (MODIS) near-infrared channels. *Journal of Geophysical Research*, **108**(D13), p. 4389, doi:10.1029/2002JD003023, 2003.
- HANSEN, R., 2001, *Radar Interferometry: Data interpretation and error analysis* (Dordrecht: Kluwer Academic Publishers).
- LI, Z., MULLER, J.-P. and CROSS, P., 2003, Comparison of precipitable water vapor derived from radiosonde, GPS, and Moderate-Resolution Imaging Spectroradiometer measurements. *Journal of Geophysical Research*, **108**(D20), p. 4651, doi:10.1029/2003JD003372.
- LI, Z., MULLER, J.-P., CROSS, P. and FIELDING, E., 2005, Interferometric synthetic aperture radar (InSAR) atmospheric correction: GPS, Moderate Resolution Imaging Spectroradiometer (MODIS), and InSAR integration. *Journal of Geophysical Research*, **110**(B3), B03410, doi:10.1029/2004JB003446.
- MENZEL, W., WYLIE, D. and STRABALA, K., 1996, Seven years of global cirrus cloud statistics using HIRS. In *IRS 1996 Symposium: Current Problems in Atmospheric Radiation*, W.L. Smith and K. Stamnes (Eds), *Proceedings of the International Radiation Symposium*, Fairbanks, Alaska, 19–24 August 1996 (Hampton, Virginia: Deepak Publishing), pp. 719–725.
- NIELL, A., COSTER, A., SOLHEIM, F., MENDES, V., TOOR, P., LANGLEY, R. and UPHAM, C., 2001, Comparison of measurements of atmospheric wet delay by radiosonde, water vapor radiometer, GPS, and VLBI. *Journal of Atmospheric and Oceanic Technology*, **18**, pp. 830–850.
- REIGBER, C., GENDT, G., DICK, G. and TOMASSINI, M., 2002, Near-real-time water vapor monitoring for weather forecasts. *GPS World*, January 2002, pp. 18–27.
- ROSEN, P., HENSLEY, S., JOUGHIN, I., LI, F., MADSEN, S., RODRIGUEZ, E. and GOLDSTEIN, R., 2000, Synthetic aperture radar interferometry—Invited paper. *Proceedings of the IEEE*, **88**, pp. 333–382.

- WILLIAMS, S., BOCK, Y. and FANG, P., 1998, Integrated satellite interferometry: troposphere noise, GPS estimates, and implications for synthetic aperture radar products. *Journal of Geophysical Research*, **103**, pp. 27051–27067.
- WYLIE, D. and MENZEL, W., 1999, Eight years of high cloud statistics using HIRS. *Journal of Climate*, **12**, pp. 170–184.
- ZEBKER, H. and VILLASENOR, J., 1992, Decorrelation in interferometric radar echoes. *IEEE Transactions on Geoscience and Remote Sensing*, **30**, pp. 950–959.
- ZEBKER, H., ROSEN, P. and HENSLEY, S., 1997, Atmospheric effects in interferometric synthetic aperture radar surface deformation and topographic maps. *Journal of Geophysical Research*, **102**, pp. 7547–7563.